International Journal of Pharmaceutics 651 (2024) 123788

Contents lists available at ScienceDirect

International Journal of Pharmaceutics

journal homepage: www.elsevier.com/locate/ijpharm

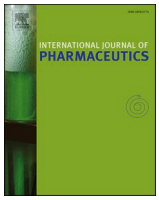

Exosome-like genistein-loaded nanoparticles developed by thin-film hydration and 3D-printed Tesla microfluidic chip: A comparative study

Maria Tsakiri [a], Atabak Ghanizadeh Tabriz [b,c], Nikolaos Naziris [a], Kanza Rahali [c], Dennis Douroumis [b,c,*], Costas Demetzos [a,*]

[a] Section of Pharmaceutical Technology, Department of Pharmacy, School of Health Sciences, National and Kapodistrian University of Athens, Panepistimioupolis Zografou 15771, Athens, Greece
[b] Delta Pharmaceutics Ltd., Chatham, Kent ME4 4TB, UK
[c] Centre for Research Innovation (CRI), University of Greenwich, Chatham Maritime, Kent ME4 4TB, UK

ARTICLE INFO

Keywords:
Exosomes
Liposomes
Microfluidics
3D printing
Nanoparticles

ABSTRACT

Exosomes are naturally derived information carriers that present interest as drug delivery systems. However, their vague cargo and isolation difficulties hinder their use in clinical practice. To overcome these limitations, we developed exosome-like nanoparticles, consisted of the main lipids of exosomes, using two distinct methods: thin-film hydration and 3D-printed microfluidics. Our novel microfluidic device, fabricated through digital light processing printing, demonstrated a favorable architecture to produce exosome-like nanoparticles. We compared these two techniques by analyzing the physicochemical characteristics (size, size distribution, and ζ-potential) of both unloaded and genistein-loaded exosome-like nanoparticles, using dynamic and electrophoretic light scattering. Our findings revealed that the presence of small lipophilic molecules, cholesterol and/or genistein, influenced the characteristics of the final formulations differently based on the development approach. Regardless of the initial differences of the formulations, all exosome-like nanoparticles, whether loaded with genistein or not, exhibited remarkable colloidal stability over time. Furthermore, an encapsulation efficiency of over 87% for genistein was achieved in all cases. Additionally, thermal analysis uncovered the presence of metastable phases within the membranes, which could impact the drug delivery efficiency. In summary, this study provides a comprehensive comparison between conventional and innovative methods for producing complex liposomal nanosystems, exemplified by exosome-like nanoparticles.

1. Introduction

Nanomedicine is an emerging field that has significantly contributed to the development of novel medicines during the last decades (Germain et al., 2020; Martins et al., 2020). The production of biocompatible nanocarriers which can protect sensitive active pharmaceutical ingredients (APIs) and deliver them precisely to a pathologic tissue eliminates the systemic adverse effects of the API and opens new horizons in modern therapy and diagnosis (Aminu et al., 2020; Sahu et al., 2021; Thapa and Kim, 2023). Since the approval of the first nanoparticulated medicine in 1995 (Barenholz, 2012), many more have been marketted (Anselmo and Mitragotri, 2019; Thapa and Kim, 2023). In many cases, nanomedicines improve the quality of life of the patient, especially when a demanding medication is required (Anderson et al., 2020; Eskandari et al., 2020; Uppal et al., 2018). Not surprisingly, most recently, the progress in the field of pharmaceutical nanotechnology led to the development and approval of the COVID-19 vaccines (Tsakiri et al., 2021).

Drug delivery nanosystems are divided into various groups based on their components i.e., lipidic, polymeric, or metallic nanoparticles (Afzal et al., 2022). Lipid nanoparticles are the most promising ones, as they present the highest biocompatibility and lowest toxicity among the other materials (Mitchell et al., 2021; Sercombe et al., 2015). A variety of biomaterials that are present in eukaryotic cellular membranes, such as phospholipids and cholesterol, are usually the basic components of lipid nanoparticles allowing the degradation of the nanoplatform and the release of the API without causing any toxic effect (Mitchell et al., 2021). Based on the above properties, many research groups have worked on the design of biomimetic lipid drug delivery nanoplatforms that present remarkable results (Leung et al., 2015; Sarfraz et al., 2018;

* Corresponding authors.
E-mail addresses: demetzos@pharm.uoa.gr (D. Douroumis), D.Douroumis@gre.ac.uk (C. Demetzos).

https://doi.org/10.1016/j.ijpharm.2024.123788
Received 20 September 2023; Received in revised form 18 December 2023; Accepted 4 January 2024
Available online 6 January 2024

Vhora et al., 2019).

Exosomes are naturally derived information delivery nanosystems (40–160 nm) as they promote inter- and intra-cellular communication. They are carriers of a plethora of different biomolecules such as proteins and peptides, nucleic acids, and lipids (Kalluri and LeBleu, 2020; Théry et al., 2002; Tsakiri et al., 2022a). Currently, exosomes are studied as novel advanced therapeutic medicinal products and according to clinicaltrials.gov, 25clinical studies concerning exosomes as therapeutic delivery systems are active today. The structure of their lipid membrane is the main parameter that allows exosomes to be present in circulation for a long period without activating phagocytosis mechanisms (Das et al., 2019). Their membranes' physicochemical and morphological characteristics are of high interest in the field of pharmaceutical technology (Skotland et al., 2017). Nevertheless, exosomes are inherently heterogeneous particles, posing challenges in precise cargo control as their content closely mirrors the intracellular contents of the parent cell. (Aryani and Denecke, 2016; Tsakiri et al., 2022a). Genetic modifications of the parent cells and/or post-production modifications are necessary procedures for the utilization of exosomes as advanced medicinal products (Aday et al., 2021). According to the above, the design of exosome-like particles that mimic the exosomal membrane properties but lack their complex content could lead to the development of safe and efficient drug or biomolecule delivery nanoplatforms (García-Manrique et al., 2018; Li et al., 2021).

The utilization of microfluidic devices for the development of soft-matter drug delivery nanoparticles is an easy, one-step, scalable process that gains ground upon other classic manufacturing procedures. For instance, this method eliminates the presence of toxic organic solvents i.e., chloroform that are extensively used in popular methods, such as thin film hydration. Moreover, additional steps for the homogenization and optimization of the nanocarriers, such as sonication or extrusion are not required (Ahn et al., 2018; Aranguren et al., 2020; Karnik et al., 2008; Leung et al., 2015; Zhao, 2013). By adjusting the critical mechanical properties of the microfluidic device someone can control and optimize the production of the lipid nanoparticles (Waghule et al., 2023). The architecture of the device and the width and length of the channels are the constant mechanical parameters that affect the characteristics of a lipid nanoparticulated formulation, while the total flow rate (TFR) and the flow rate ratio (FRR) are the variable parameters in the mentioned procedure (Rebollo et al., 2022; Roces et al., 2020).

Although the microfluidic technique is unquestionably a novel method for the production of such innovative nanoplatforms, currently, it is usually accompanied by high cost of the equipment and limitations in the flexibility of the device architecture (Chakraborty and Parvez, 2022; Elvira, 2021). The above limitations can be overcome by the ground-breaking evolution of additive manufacturing (Wang et al., 2020). Three-dimensional printing allows the facile cost-effective design and development of complex microfluidic device architectures, according to the specific needs of each project (Tiboni et al., 2021). Many types of printers have been studied for this purpose. Weaver et al. used a liquid crystal display printer to develop their devices, while Sommonte et al., preferred to print their "diamond shaped" chips with a digital light processing (DLP) printer (Sommonte et al., 2022; Weaver et al., 2023).

The aim of the present study is the comparison of a microfluidic technique via the use of a 3d-printed device to a classic, thin film hydration-sonication approach for the development of exosome-like nanoparticles. For this purpose, different molar ratios of 1,2-dipalmitoyl-*sn*-glycero-3-phosphocholine (DPPC), Sphingomyelin (Egg, Chicken) (SM), 1,2-dioleoyl-*sn*-glycero-3-phospho-L-serine (PS 18:0/18:1 or DOPS) and cholesterol (Chol) were used. Genistein, an isoflavone with anti-inflammatory and antioxidant activity was used as a model small drug molecule. The microfluidic device was developed by DLP printing and the optimum TFR and FRR for the production of the exosome-like nanoparticles were selected. The physicochemical characteristics (hydrodynamic diameter, polydispersity index, and ζ-potential) of both the formulations developed by thin film hydration-sonication and by the microfluidic device were studied by dynamic and electrophoretic light scattering. Moreover, we evaluated the incorporation efficiency of genistein. Finally, the lipid membranes of the present formulations were analyzed by differential scanning calorimetry.

2. Methods and materials

2.1. Materials

1,2-dipalmitoyl-*sn*-glycero-3-phosphocholine (DPPC), Sphingomyelin (Egg, Chicken) (SM) were purchased from Avanti® Polar Lipids Inc. (Alabaster, AL, USA).1,2-dioleoyl-*sn*-glycero-3-phospho-L-serine (PS 18:0/18:1 or DOPS) was received as a gift from Lipoid GmbH (Ludwigshafen, Germany). Cholesterol and genistein were acquired from Sigma-Aldrich Chemical Co. (St. Louis, MO, USA). Chloroform, ethanol, acetone and HPLC-grade water were of analytical grade and purchased from Sigma-Aldrich® Co. (St. Louis, MO, USA). The Microfluidic chips were 3D-printed using microfluidic resin, MiiCraft BV-007A (Young Optics Inc., Hsinchu, Taiwan).

2.2. Design and 3D printing of microfluidic chip

Microfluidic chip was designed via CAD software (SolidWorks 2018–2019, Dassault Systèmes). The Chip comprises of two large threaded inlets as showing in Fig. 1 designed with 8 mm length at 28 threads per inch. Each large inlet converges into an independent rectangular inlet channek with a width of 500 μm and a height of 300 μm. Both inlets then merge into larger mixing channel with identical height and a width of 800 μm and a channel length of 3.5 cm followed by an outlet. Within the length of the mixing channel, fin like structures is present with repeated patterns (32 cycles). The fins dimensions within a single cycle are shown in Fig. 2. Each fin's thickness is approximately 100 μm.

The chip was 3D printed using a DLP based printed Asiga Max equipped with a 385 nm UltraViolet (UV) DLP projector with pixel size at 27 μm. A low viscosity microfluidic resin was used for 3D printing of the microfluidic chips. The designed.prt file was then converted in to a stl file a readable file compatible with printer's slicing software Composer (Composer 2.1, Asiga). The structure was then laid flat on the build plate for the slicing. The Chip was sliced at 25 um layer thickness with no support needed. Each layer of the chip was printed using a UV intensity of 3 mW/cm^2 and a layer exposure time of 3.3 s accordingly. First layer exposure time was set to 112 s with identical UV intensity to ensure adequate adherence of the chip to the build plate.

After completion of the printing process the chip was gently removed from the build plate and then immersed in isopropanol bath for 10 min to wash out any uncured resin residues on the surface of the microfluidic chip. The internal channels then were washed for 5 cycles with isopropanol to wash away the uncured resin residues within the microfluidic channels. The chip was left for 4 h or overnight at ambient environment to dry. At the end the chip was cured under optimised settings from previous studies in a UV-A heated chamber at 40 °C for 60 min to complete the polymerization of the microfluidic chip (Tabriz et al., 2022).

2.3. Preparation of liposomes by thin film hydration (TFH) method

Liposomes were prepared according to the thin-film hydration method reported in the literature at a concentration equal to 10 mg/mL (Tsakiri et al., 2022b). Briefly, stock solutions of DPPC, SM, DOPS, cholesterol and genistein in chloroform at a concentration 10 mg/mL were prepared (Fig. 1). Aliquots of the stock solutions were mixed into a round-bottom flask (50 mL) to prepare the exosome-like nanoparticles of the following consistency: DPPC:SM:DOPS:Chol 77.5:10:2.5:10, 75:10:5:10, 70:10:10:10, 65:10:15:10, 47.5:10:2.5:40, 45:10:5:40,

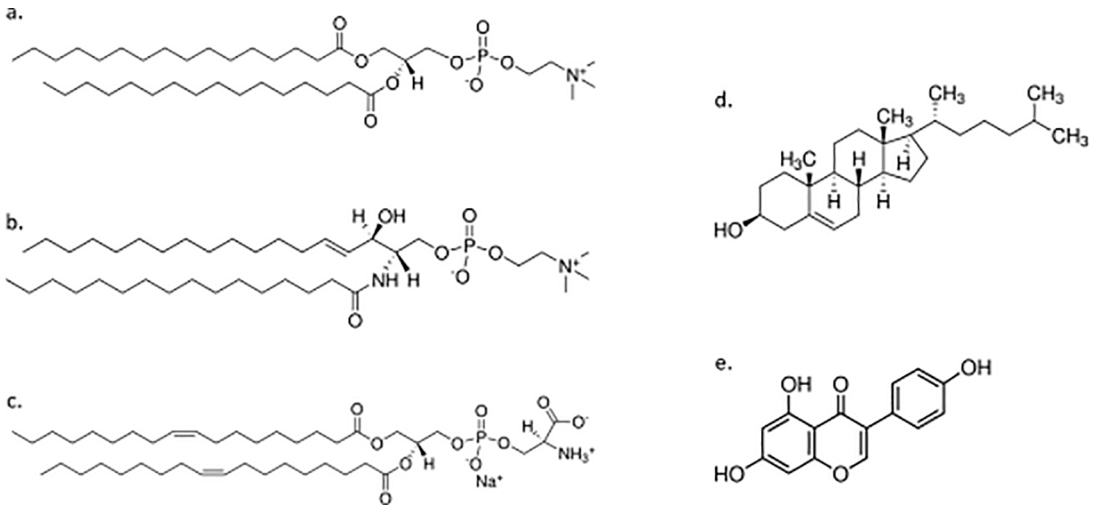

Fig. 1. The chemical structures of **a.** DPPC, **b.** SM, **c.** DOPS, **d.** cholesterol and **e.** genistein.

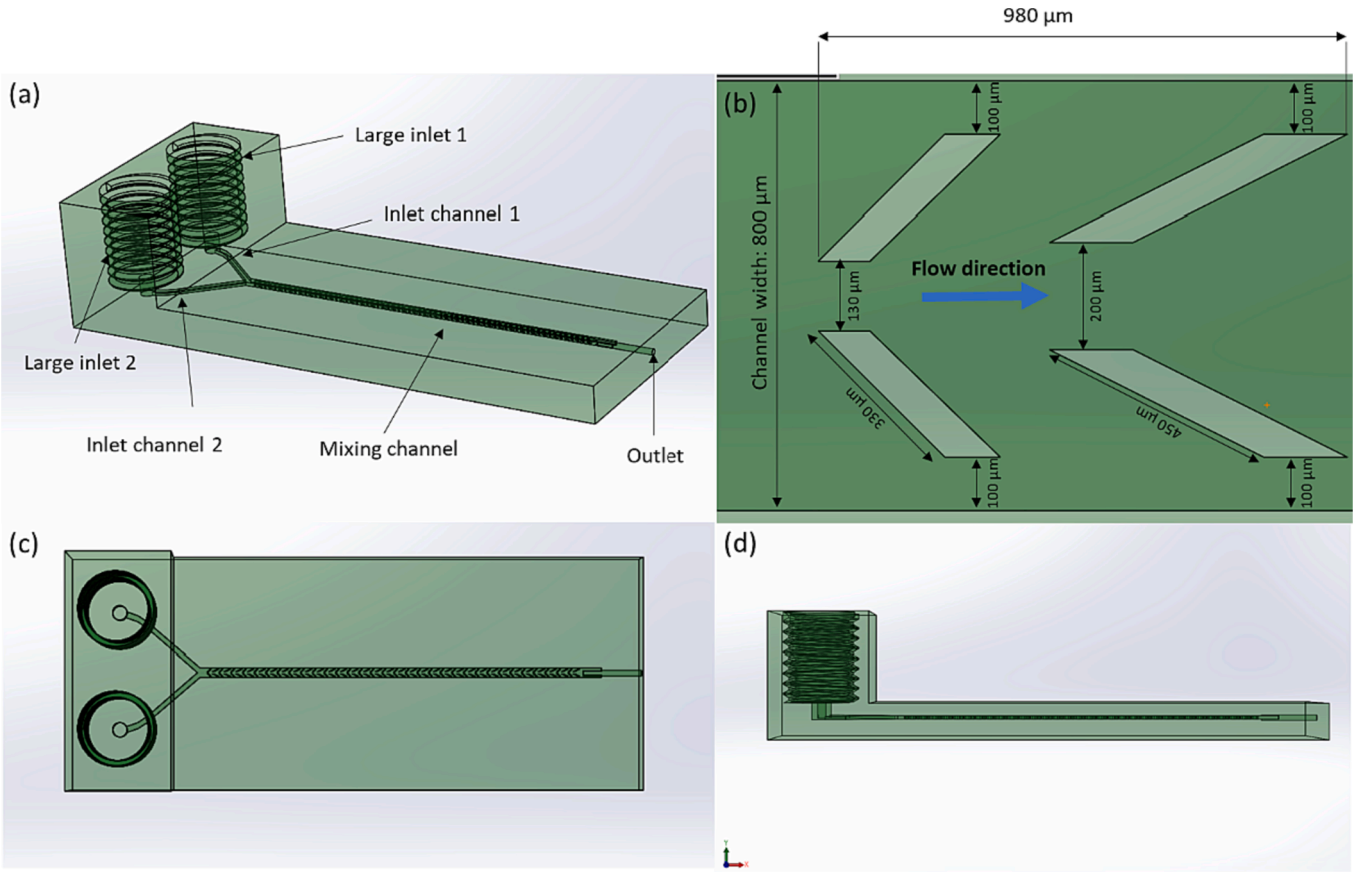

Fig. 2. **(a)** Design of the microfluidic chip. **(b)** A single cycle of the fins presents within the missing channel. **(c)** Top and **(d)** side of the microfluidic chip design.

40:10:10:40, 35:10:15:40 M ratio, and DPPC:SM:DOPS:Chol:Gen 35:10:15:35:5 and 35:10:15:30:10. The flask was inserted into a rotary evaporator (Rotavapor) and vacuum was applied at 42 °C for 30 min in order for the organic solvent to be evaporated and a thin film to be formed. The hydration process was taken place by slowly stirring for 1 h, in a temperature above the systems' phase transition temperature. The lipidic vesicle dispersions were subjected to two, 5 min sonication cycles (amplitude 70, cycle 0.5) interrupted by a 5 min resting period, in water bath, using a probe sonicator (UP 200S, dr. hielsher GmbH, Berlin, Germany). The resultant exosomes-like nanoparticles were allowed to anneal for 30 min. The final formulations were stored at 4 °C.

2.4. Microfluidic formulation of the exosomes-like nanoparticles

For the preparation of the same exosome-like nanoparticles by microfluidics, the 3D printed chip was connected to anIPS 14R independent dual channel syringe pump (Inovenso Ltd. Co, Turkey). The appropriate aliquots of DPPC, SM, DOPS, Chol and Gen (Fig. 1) were dissolved in ethanol:acetone 95:5 at a total lipid concentration 40 mg/mL. The organic phase was pumped against HPLC grade water at

controlled flow rate and the final formulations were collected from the outlet of the chip. The final concentration was 10 mg/mL. The TFR was 3 mL/min and the FRR was 6:4 (organic phase:water). The organic solvent was evaporated under a stream of argon gas and gentile magnetic stirring.

2.5. Dynamic and electrophoretic light scattering

The size, size distribution, and ζ-potential of the developed nanosystems in aqueous media were measured by dynamic light scattering (DLS) and electrophoretic light scattering (ELS). For these studies, 50 μL of the dispersion was diluted to 1 mL of HPLC-grade water and measured for particle size (hydrodynamic diameter, D_h), size distribution (polydispersity index, PDI), and charge (ζ-potential, ζ-pot). Measurements were performed at a detection angle of 90° and at 25 °C, in a photon correlation spectrometer (Zetasizer ZSU3105, Malvern, UK) and analyzed by the ZS XPLORER software (Malvern software). According to the instruments specifications, a mean count rate 200–500 kcps is optimal for the measurements. All the measurements that are presented appear a mean count rate (scattering intensity) of this range.

2.6. Entrapment efficiency (%EE) determination

The free genistein was separated from the genistein entrapped in the exosomes-like nanoparticles using the ultrafiltration centrifugal method. Briefly, the dispersion was centrifuged for 30 min at 8000 rpm using centrifugal filter tubes (molecular weight (MW) cutoff = 10 kDa; Millipore) at 4 °C. The nanoparticles were separated from the aqueous phase, and the free genistein was analyzed in the supernatant. The UV − Vis spectrophotometry method was used to measure the free drug concentration in the samples after centrifugation and supernatant collection. The absorption measurements were performed at a wavelength of 370 nm after adding 50 μL $AlCl_3$, by using UV − Vis spectrophotometry (microplate spectrophotometer INNO, LTEK Co. Ltd, Republic of Korea) and a preconstructed calibration curve. $AlCl_3$ was added to the dispersion to facilitate the quantification of genistein. Centrifuged samples of the respective empty exosome-like nanoparticles were used as a blank. The Entrapment Efficiency (%EE) was calculated according to the following equation:

$$(\%EE) = \left(1 - \frac{C_{supernatant}}{C_{total}}\right)\%$$

where $C_{supernatant}$ is the genistein concentration that was quantified in the supernatant (not entrapped) and C_{total} is the total concentration of the genistein added in the dispersion.

2.7. Differential scanning calorimetry

Differential Scanning Calorimetry experiments were performed with a DSC822e (Mettler-Toledo, Schwerzenbach, Switzerland) calorimeter, calibrated with pure indium (Tm = 156.6 °C). Sealed aluminum crucibles of 40 μL capacity were used as sample holders. Lipid bilayers of DPPC, DPPC:SM 90:10, DPPC:SM:DOPS 75:10:15, DPPC:SM:DOPS:Chol 70:10:15:5 and 65:10:15:10 as well as DPPC:SM:DOPS:Gen 70:10:15:5 and 65:10:15:10 M ratio were prepared by mixing the appropriate aliquots of the stock solutions into a round-bottom flask inserted into a rotary evaporator (Rotavapor) and vacuum was applied at 42 °C for 30 min in order for the organic solvent to be evaporated and a thin film to be formed.. The film was maintained under vacuum for at least 24 h in a desiccator to remove traces of solvent. The prepared bilayers were analyzed by placing approximately 2.0 mg of each sample in the crucible, hydrating by 50 % w/vof HPLC-grade water.

2.8. Scanning electron microscopy (SEM)

Opened designs of the microfluidic devices were printed using the same technique and the same features and SEM images were captured with Hitachi SU8030 (Tokyo, Japan) by an electron beam accelerating voltage of 1.0 kV and magnification of 30 x.

2.9. Statistical analysis

All results are expressed as mean value ± SD (SD stands for standard deviation) from three independent experiments. Most data were analyzed by using one-way ANOVA followed by Holm-Bonferroni post hoc test (unless another approach is mentioned in the graphs). When more factors were compared two-way ANOVA was performed. The significance of comparisons is presented on the graphs (*: $p < 0.05$, **: $p < 0.01$, ***: $p < 0.001$, ****: $p < 0.0001$).

3. Results and discussion

3.1. Microfluidics chip development

Microfluidic arrays have demonstrated excellent benefits for the engineering of lipid nanoparticles (Zhang et al., 2020). One alternative manufacturing technique for microfluidic chips that has lately gained popularity is 3D printing, as it has the potential to solve many issues of the poly(dimethylsiloxane) fabricated devices (Chen et al., 2016). The major advantage of 3D printing is the fabrication of robust and complex designs with unique features. In this study, the use of DLP offered excellent print resolution and enabled the printing of the designed chips. The present microfluidic chip was inspired by the one-way valve called "valvular conduit" designed by Nicola Tesla (Tesla, 1920). As shown in Fig. 2**.b** the chips are equipped with micromixer structures which create diverging flow resulting in increased pressure along the flow of the organic and aqueous phase during mixing. The pressure is called adverse pressure gradient condition. By adjusting the angle of the micromixer structures, it possible to create flow vortices that result in energy loss while the flow is divide in two part. The micromixer elements are placed in such way that the secondary flow is mixed with the primary and the process is repeated at every unit of the four micromixers. As shown in Fig. 2**.b** the distance of the first two micromixers is narrower compared to the following two of the unit and positioned at different angles so they increase the generated pressure. The mixed primary and secondary flow create chaotic advection leading to rapid mixing and the formation of nanoparticles with small particle size and narrow polydispersity index.

A major advantage of the Tesla microfluidic chip is that the width, depth, heigh and angles can be rearranged for further optimization of the design. Fig. 3 illustrates the SEM analysis of printed Tesla chips with excellent print orientation and accuracy. As shown in Fig. 3**.a** the micromixer structures are perfectly printed with distinct layers (six) and thickness of 25 μm each. Furthermore, Fig. 3**.b** shows the high precision printing of the repeated micromixer units with the exact length, width and interdistances between each fin and the microchannel walls. More importantly there are no print defects or resin residues within the microchannel that could affect the mixing of the flow streams.

3.2. Non-loaded exosome-like particles developed by Tesla microfluidic chips

Based on previous lipidomics analysis of biologically-derived exosomes (Skotland et al., 2017; Trajkovic et al., 2008), DPPC:SM:DOPS:Chol 77.5:10:2.5:10, 75:10:5:10, 70:10:10:10, 65:10:15:10 M ratio and 47.5:10:2.5:40, 45:10:5:40, 40:10:10:40, 35:10:15:40 M ratio exosome-like particles were developed. Those containing 40 % mol Chol are those presenting the high affinity to the lipid consistency of the exosomal membrane while the nanoparticles with 10 % mol of Chol are used as reference systems. We used dynamic and electrophoretic light scattering

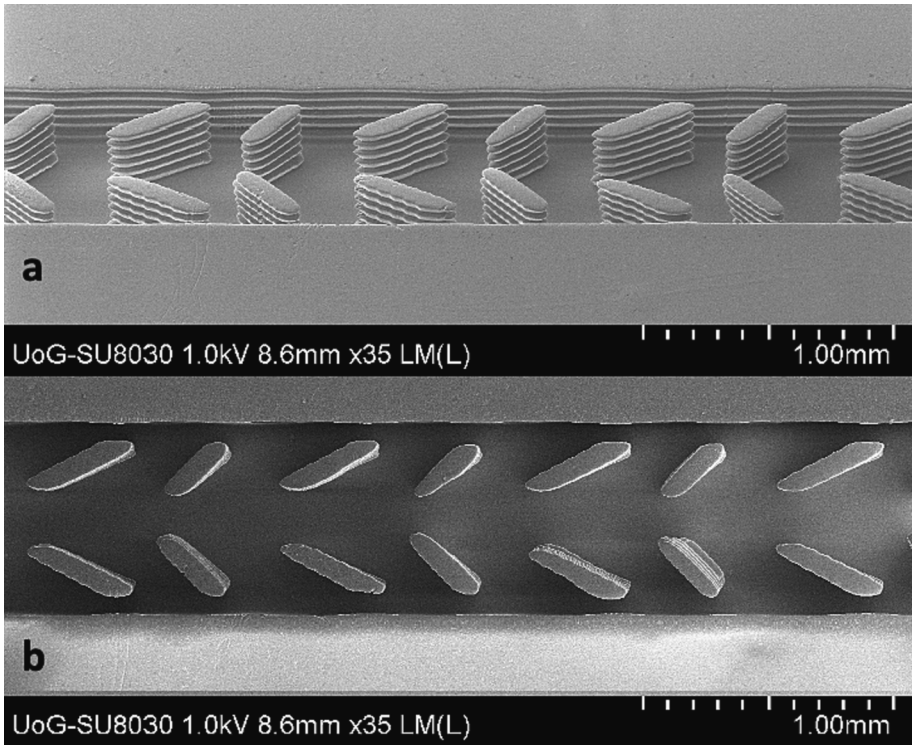

Fig. 3. SEM images of 3D printed Tesla chips.

to investigate the physicochemical characteristics of the exosome-like nanoparticles produced by the Tesla microfluidic chip. In **Figure S.1,** the size, size distribution, and ζ-potential of the prepared systems are shown.

According to the literature, although high flow rate ratios result in the formation of smaller size particles, they present some limitations associated with the physical properties of the continuous (in this case the aqueous) and the disperse (ethanolic) phase as well as with the architecture of the device. These parameters result in a maximum actual flow ratio that might be lower than the nominal one when the second is high (Costa et al., 2017). Thus, for the preparation of our formulations, we decided to use a TFR of 3 mL/min.

Differences in the hydrodynamic diameter (D_h) and polydispersity index (PDI) values of the developed exosome-like nanoparticles can be detected **(**Table 1**)**. A higher percentage of cholesterol leads to smaller and more homogenous drug-delivery nanosystems. Regarding the systems that contain 10 % mol Chol, the D_h values vary from approximately 150 nm to 360 nm, while values 140 to 190 nm are observed for the exosome-like particles with a higher amount of cholesterol. Cholesterol is a sterol molecule well-known for its ability to modify the rigidity/flexibility of lipid bilayers and thus, it is one of the main factors that determine the stability of liposomal formulations (Nakhaei et al., 2021). We believe that the formation of liposomal nanoparticles with optimized physicochemical characteristics in terms of size and size distribution of the systems with 40 % mol Chol is attributed to the decreased affinity of the lipid bilayer with ethanol in contrast to the systems with 10 % mol Chol (Trandum et al., 2000). Subsequently, during the mixing process of the aqueous and organic phases, the self-assembly of the lipidic bilayer fragments leads to an increase in the surface area-to-volume ratio (Antonietti and Förster, 2003).

Table 1
The physicochemical characteristics (D_h, PDI and ζ-potential) of the exosome-like particles prepared by the Tesla microfluidic chips.

System	Molar ratio	Dh (nm)	PDI	ζ-potential (mV)
10 % Chol				
DPPC:SM: DOPS:Chol	77.5:10:2.5:10	177.8 ± 4.2	0.382 ± 0.018	–33.3 ± 4.7
DPPC:SM: DOPS:Chol	75:10:5:10	155.8 ± 2.7	0.306 ± 0.012	−16.3 ± 0.2
DPPC:SM: DOPS:Chol	70:10:10:10	258.7 ± 5.0	0.428 ± 0.036	−57.8 ± 3.2
DPPC:SM: DOPS:Chol	65:10:15:10	362.3 ± 1.6	0.218 ± 0.016	−57.5 ± 1.2
40 % Chol				
DPPC:SM: DOPS:Chol	47.5:10:2.5:40	155.8 ± 0.2	0.219 ± 0.011	−30.5 ± 0.7
DPPC:SM: DOPS:Chol	45:10:5:40	141.3 ± 0.0.3	0.111 ± 0.021	−34.4 ± 0.2
DPPC:SM: DOPS:Chol	40:10:10:40	186.5 ± 0.3	0.099 ± 0.007	−57.4 ± 1.0
DPPC:SM: DOPS:Chol	35:10:15:40	140.7 ± 0.4	0.126 ± 0.004	−52.8 ± 1.4

As for the nanoparticles with the lower percentage of cholesterol, an increase in DOPS notably drives the lipids to self-assemble into larger nanoparticles while the homogeneity of the structures is improved **(**Table 1 **and Figure S.1.a)**. The observed augmentation in the hydrodynamic diameter resulting from the increase in DOPS is consistent with the results obtained by Casadó and group (Casadó et al., 2018). The present phenomenon is not observed for the exosome-like particles that consist of a higher amount of cholesterol.

In conclusion, as cholesterol affects the flexibility of the lipid membranes, we believe that the development of lipid nanoparticles by the use of microfluidic devices is preferable when the consistency of the nanosystems is rich in a rigidity/flexibility regulator such as cholesterol or a lipid with a low transition temperature from the gel phase to the liquid crystalline phase.

Regarding the absolute ζ-potential value of the empty exosome-like nanoparticles, an increase is observed as the % mol DOPS increases. The above is attributed to the negative charge of the DOPS lipid **(Figure S.1.c)**. Non-significant differences are shown between the groups that contain 10 or 40 % mol Chol for all nano-formulations except of the those that contain 5 % DOPS. According to the literature

(Demetzos, 2016), nanoparticles with ζ-potential values exceeding 30 mV exhibit long-term physicochemical stability. Almost all the exosome-like nanoparticles we received surpass this 30 mV threshold.

As shown in Fig. 4, the long-term physicochemical stability of the developed nanoplatforms is verified by the obtained results. No ΔD_h higher than 30 nm is detected and PDI values are not significantly affected after 7 days. A significant increase of the PDI, when compared to the value of the day of production, can be detected mainly for the exosome-like particles that consist of 10 % Chol. Except of their smaller hydrodynamic diameter, the exosome-like particles with 40 % Chol presented lower PDI values, too.

3.3. Non-loaded exosome-like particles developed by thin film hydration-sonication method

To compare the efficiency of microfluidic and thin film hydration-sonication methods, we developed the same exosome-like nanoparticles DPPC:SM:DOPS:Chol 77.5:10:2.5:10, 75:10:5:10, 70:10:10:10, 65:10:15:10 and 47.5:10:2.5:40, 45:10:5:40, 40:10:10:40, 35:10:15:40- by the thin film hydration method. Subsequently, a sonication protocol was followed for the decrease of the size and size distribution of the formulations. The hydrodynamic diameter (D_h) and polydispersity index (PDI) of the platforms were evaluated by DLS measurements while the ζ-potential value was calculated by ELS.

Figure S.2 and Table 2, present the D_h, PDI and ζ-potential values of freshly prepared exosome-like nanoparticles. For the compositions with 10 % mol Chol, the size was not significantly affected by the increase of DOPS – all the D_h values range between 48.4 and 59.8 nm. As for the exosome-like nanoparticles consisted of 40 % mol Chol, the D_h values varied from 70.8 to 82.9 nm. The findings indicate that higher Chol amounts resulted in increased liposome sizes by approximately 20 nm (**Figure S.2**) which are in accordance with previous studies (Kaddeh et al., 2018). This is due to the Chol effect which acts as a membrane fluidity modulator. Specifically, we believe that high ratio of Chol results in a limit of the particle's curvature, and in this way, prohibiting the formation of exosome-like particles of a lower hydrodynamic diameter. However, the increase in the size of the exosome-like nanoparticles is not accompanied by an increase in the polydispersity index as the PDI values remain stable at approximately 0.3 in all cases.

Due to the negative charge of the DOPS head group, the platforms

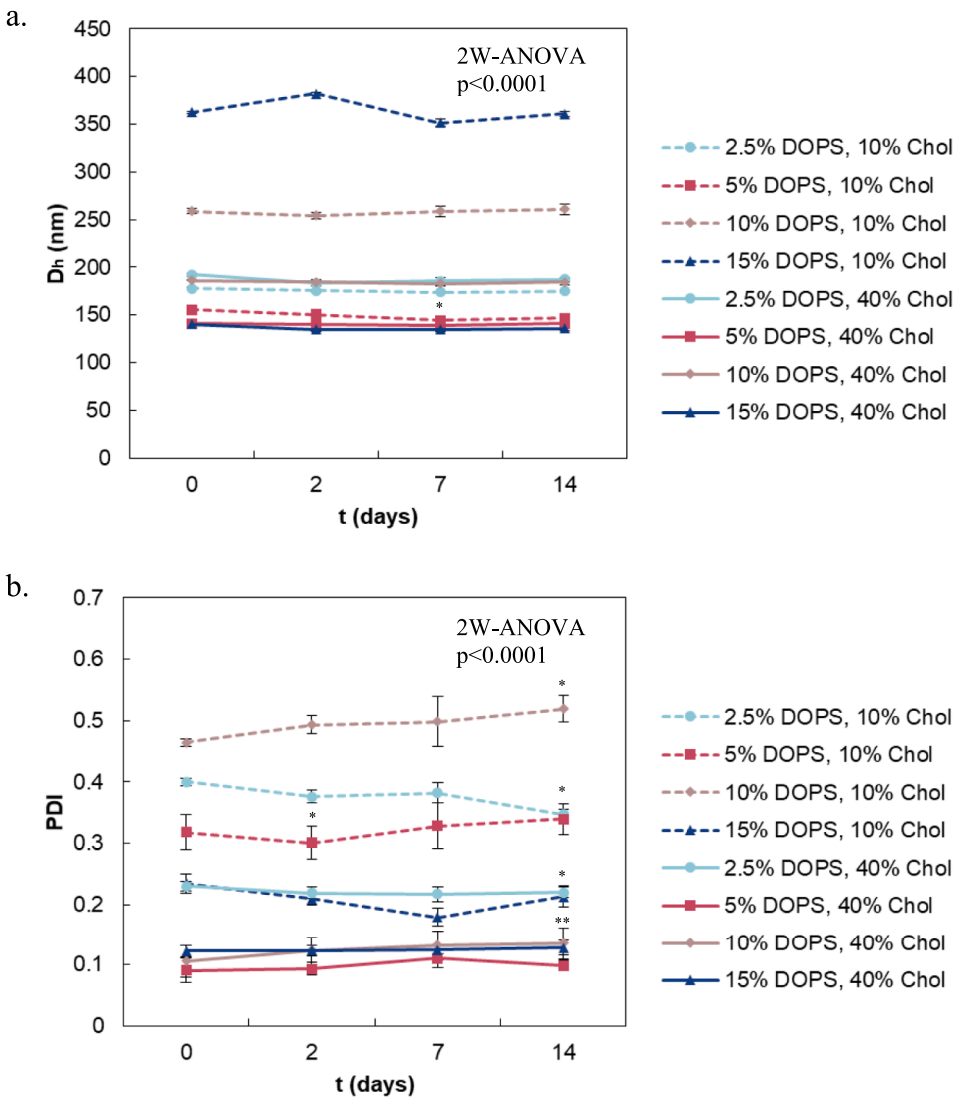

Fig. 4. Stability assessments of **a.** the size (Dh, nm) and **b.** the polydispersity index (PDI) of DPPC:SM:DOPS:Chol 77.5:10:2.5:10, 75:10:5:10, 70:10:10:10, 65:10:15:10 M ratio and 47.5:10:2.5:40, 45:10:5:40, 40:10:10:40, 35:10:15:40 M ratio exosome-like particles, developed by the Tesla microfluidic chips. Data are presented as mean value ± SD (n = 3). Significance of the effect of lipid composition on the stability was studied by 2 W-ANOVA. To determine the stability over time (days 2,7, and 14 versus day 0) of each formulation student *t*-test was used (significant values are reported in the figures; *: $p \leq 0.05$, **: $p \leq 0.01$).

Table 2
The physicochemical characteristics (D_h, PDI and ζ-potential) of the exosome-like particles prepared by thin film hydration-sonication method.

System	Molar ratio	Dh (nm)	PDI	ζ-potential (mV)
10 % Chol				
DPPC:SM:DOPS: Chol	77.5:10:2.5:10	48.4 ± 9.0	0.297 ± 0.055	−20.1 ± 1.1
DPPC:SM:DOPS: Chol	75:10:5:10	56.3 ± 10.4	0.318 ± 0.068	−31.7 ± 1.9
DPPC:SM:DOPS: Chol	70:10:10:10	59.8 ± 7.3	0.279 ± 0.013	−54.5 ± 2.3
DPPC:SM:DOPS: Chol	65:10:15:10	58.5 ± 11.8	0.316 ± 0.048	−64.7 ± 2.9
40 % Chol				
DPPC:SM:DOPS: Chol	47.5:10:2.5:40	70.8 ± 9.1	0.260 ± 0.068	−21.5 ± 2.6
DPPC:SM:DOPS: Chol	45:10:5:40	79.0 ± 10.6	0.270 ± 0.039	−52.0 ± 2.7
DPPC:SM:DOPS: Chol	40:10:10:40	78.5 ± 14.4	0.298 ± 0.044	−54.7 ± 1.7
DPPC:SM:DOPS: Chol	35:10:15:40	82.9 ± 11.8	0.303 ± 0.068	−50.2 ± 2.3

appear to have negative ζ-potential values. As expected, increasing the ratio of DOPS causes more negative values. Interestingly, the system that contains 5 % DOPS mol and a higher ratio of Chol (40 %) present slightly more negative values in comparison with the one that consists of 10 % mol Chol. The above is in accordance with the studies of Magarkar et al, who pointed out that increasing level of Chol decreases the ability of Na^+ ions to interact with negatively charged areas of the phosphatidylcholines (PCs) using molecular dynamics simulation and experimental data (Magarkar et al., 2014). However, this effect is not observed in systems with a higher percentage of DOPS molecules, suggesting that in such cases, the mentioned effect is insignificant.

Regarding the physicochemical stability of the exosome-like nanoparticles over time **(**Fig. 5**)**, it was shown that neither the size nor the polydispersity of the platforms undergoes any changes after 15 days. However, the lipid consistency of the exosome-like particles significantly affects the hydrodynamic diameter and the polydispersity index of the nano-formulations. The exosome-like nanoparticles that present the lowest stability over this period are the ones that consist of 5 % mol DOPS and 40 % mol Chol ($\Delta D_h = 12.3$ nm). Monodisperse graph populations (PDI values between 0.3 and 0.4) are received for all the systems and no aggregation trends are observed. Thus, we assume that the electrostatic repulsions caused by even the lowest consistency of DOPS (2.5 % mol), when the ζ-potential value is approximate –20 mV, are capable to retain the nanoparticle stability over this period.

3.4. Entrapment of genistein into the exosome-like particles

Genistein is an isoflavone molecule with anti-inflammatory and antioxidant activity. The role of genistein as a neuroprotective molecule has been widely evaluated (Mas-Bargues et al., 2022; Seo et al., 2018; Petry et al., 2021; Hirohata et al., 2012). Nevertheless, due to it's physicochemical characteristics, limited bioavailability has been issued (Gleason et al., 2015).

For the development of the genistein-loaded nanoplatforms, we proceeded with the formulations that contain 40 % mol of the small lipophilic molecules (cholesterol and/or genistein), which are incorporated in the lipidic membrane. Thus, we designed and developed DPPC:SM:DOPS:Chol:Gen 35:10:15:35:5 (G-1) and 35:10:15:30:10 (G-2), exosome-like particles which contained 5 % and 10 % of genistein respectively.

As shown in Fig. 6**,** regarding the particle size of the genistein-loaded exosome-like nanoparticles, prepared by the thin-film hydration method, the replacement of a cholesterol part to a genistein part causes a decrease of the particles' size and polydispersity index. However, it appears that the obtained particle size (~60 nm) was not affected by the ratio of genistein (5 to 10 %). In contrast, as to the Tesla chips, the increased genistein amounts led to larger particle size and PDI of the exosome-like nanoparticles. In fact, by increasing the ratio of genistein from 5 to 10 %, the particle size was significantly increased to 340 nm for the latter. The homogeneity of these particles in this case is higher for the G-2 systems (10 % mol genistein). The 14-day stability assessment showed that the formulations developed either by thin-film hydration/sonication or by microfluidic device retained the physicochemical characteristics (size and polydispersity).

The % entrapment efficiency (%EE) of genistein was measured by UV–Vis spectrophotometry. As genistein is a molecule with a water solubility lower than 1 μg/ml (Cohen et al., 2011), high incorporation ratio is expected. Indeed, the obtained data revealed a %EE higher than 87 % in all the cases **(Figure S.3)**. The exosome-like particles received by the microfluidics technique presented slightly increased %EE values when compared to the ones developed by the thin-film hydration/sonication method.

3.5. Comparison of the thin film hydration method and microfluidics for the development of the exosome-like particles

The comparison of thin film hydration and microfluidic techniques for the development of lipid-based nanoparticles picked out their effect on the obtained particle size. In the present work, both approaches were evaluated for the development of complex biomimetic lipid nanoparticles.

The experimental findings demonstrated that the processing technology and the lipid consistency play an important role. The usage of microfluidics chips led to nanoparticles with increased particle size which is in contrast to similar studies (Al-amin et al., 2020; Skupin-Mrugalska et al., 2021). However the results are related to the formulation complexity such as the presense of highly chargable lipids and genetic material (Elsana et al., 2019). The use of 3D-printed microfluidic chips led to the formation of nanoparticles with better polydispersity by altering the Chol ratios. Increased Chol amounts led to smaller nanoparticles and confirmed that Chol improves the packing defects of the lipid bilayers. On the other hand, TFH led to the hydrodynamic diameter).

Notably, increased ratio of DOPS led to the formation of exosome-like particles of increased hydrodynamic diameter for both methods. Regarding the PDI, in the case of the microfluidics chip, we observe similar values to the other formulations, while when we applied the TFH, increasing of DOPS resulted in analogous increase of the PDI.

The stability over time for all exosome-like nanoparticles was not influenced by the processing methodology but was dependent on the formulation composition. The experimental findings suggest that even low DOPS (2.5 %) amounts promote the nanoparticle stability.

The incorporation of the drug resulted in significant differences on the hydrodynamic diameter and the polydispersity index of the formed nanoparticles. While the stability is maintained for all the formulations, when the 3D-printed chips were used, increasing ratio of genistein led to a significant increase of the hydrodynamic diameter of the dispersion. To the contrary, for the TFH-sonication technique the incorporation of higher genistein amounts has not caused any remarkable effects on the exosome-like nanoparticles characteristics. The slightly higher %EE that was obtained by using microfluidics chips, in comparison to previous studies (Al-amin et al., 2020), suggests that the technology can facilitate better encapsulation efficiency for hydrophobic molecules.

3.6. Thermotropic behavior of the exosome-like membranes

The thermotropic behavior of DPPC, DPPC:SM 90:10, DPPC:SM:DOPS 75:10:15, DPPC:SM:DOPS:Chol 70:10:15:5 and 65:10:15:10 as well as DPPC:SM:DOPS:Gen 70:10:15:5 and 65:10:15:10 M ratio was evaluated by DSC (Fig. 7 **and** Table 3**)**. The analysis is based on T_{onset},

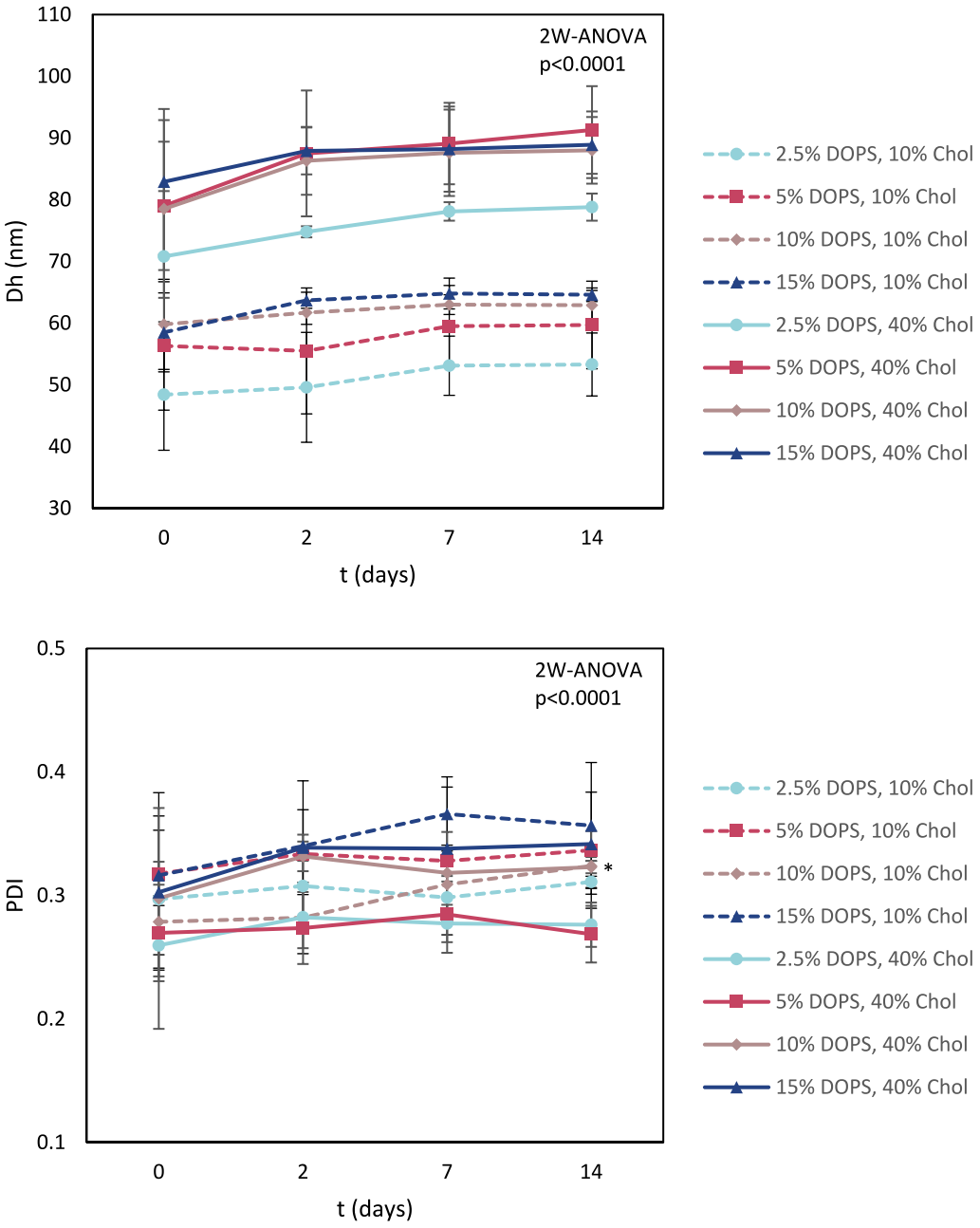

Fig. 5. Stability assessments of **a.** the size (Dh, nm) and **b.** the polydispersity index (PDI) of DPPC:SM:DOPS:Chol 77.5:10:2.5:10, 75:10:5:10, 70:10:10:10, 65:10:15:10 M ratio and 47.5:10:2.5:40, 45:10:5:40, 40:10:10:40, 35:10:15:40 M ratio exosome-like particles, developed by thin film hydration-sonication method. Data are presented as mean value ± SD (n = 3). Significance of the effect of lipid composition on the stability was studied by 2 W-ANOVA. To determine the stability over time (days 2,7, and 14 versus day 0) of each formulation student *t*-test was used (significant values are reported in the figures; *: $p \leq 0.05$).

T_m, $\Delta T_{1/2}$, and ΔH of fully hydrated lipid bilayers which were used to investigate the effect of each biomaterial on the properties of the membrane.

As it is shown in Fig. 7**.a**, the characteristic low-enthalpy pretransition at 35.69 °C and the main sharp transition curve from the ripple phase (P_β') to the liquid crystalline phase (L_α') at 41.49 °C appear on the thermogram(Gardikis et al., 2006; Matsingou et al., 2005). When sphingomyelin (SM) is inserted in the bilayer, both the pretransition and the main curves shift to lower temperatures (29.35 °C and 39.96 °C, respectively). However, we observe an increase of the ΔH and a small decrease in the curve width ($\Delta T_{1/2}$), showing a stiffer conformation of the membrane that presents low polydispersity.

The elimination of the ripple phase (represented by the pretransition curve) and intense decrease of the main transitions' ΔH from 45.98 J/g to 27.77 J/g are observed when 15 % mol DOPS is added in the bilayer. The abolishment of the pretransition is attributed to the changes in the mobility of the DPPC choline polar heads (Gardikis et al., 2006) while the decrease of the ΔH is correlated to the mobility of the alkyl chains (Zhao et al., 2007). DOPS dispose of two mono-unsaturated alkyl chains, which weaken the hydrophobic van der Waals interactions of the interior hydrophobic area of the bilayer leading to a looser and more flexible bilayer (Leekumjorn et al., 2009). Moreover, the addition of DOPS causes a de-convolution of the main transition curve, which is more visible in the cooling process **(Figure S.4).** This phenomenon indicates the presence of two distinct lipidic composition areas, similar to the lipid rafts that appear in the cellular membrane. Lipid rafts are areas in the bilayer that are rich in saturated lipids, sphingomyelin, and cholesterol dispersed in a matrix composed of high ratios of unsaturated lipids

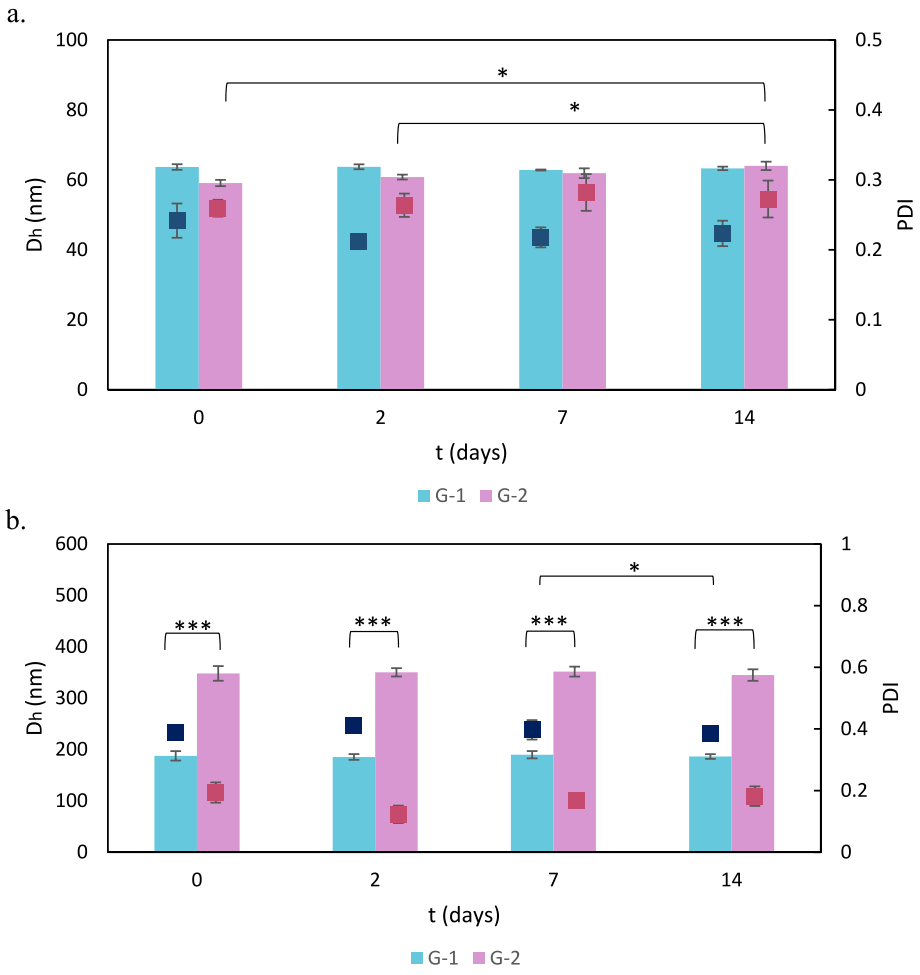

Fig. 6. Stability assessments of the size (Dh, nm) in bars and the polydispersity index (PDI) in dots of DPPC:SM:DOPS:Chol:Gen 35:10:15:35:5 (G-1) and 35:10:15:30:10 (G-2) developed by **a.** thin film hydration protocol and **b.** 3d-printed microfluidic technique. Data are presented as mean value ± SD of three independent measurements (n = 3). Significant values are reported in the figures; *: $p \leq 0.05$), ***: $p \leq 0.001$.

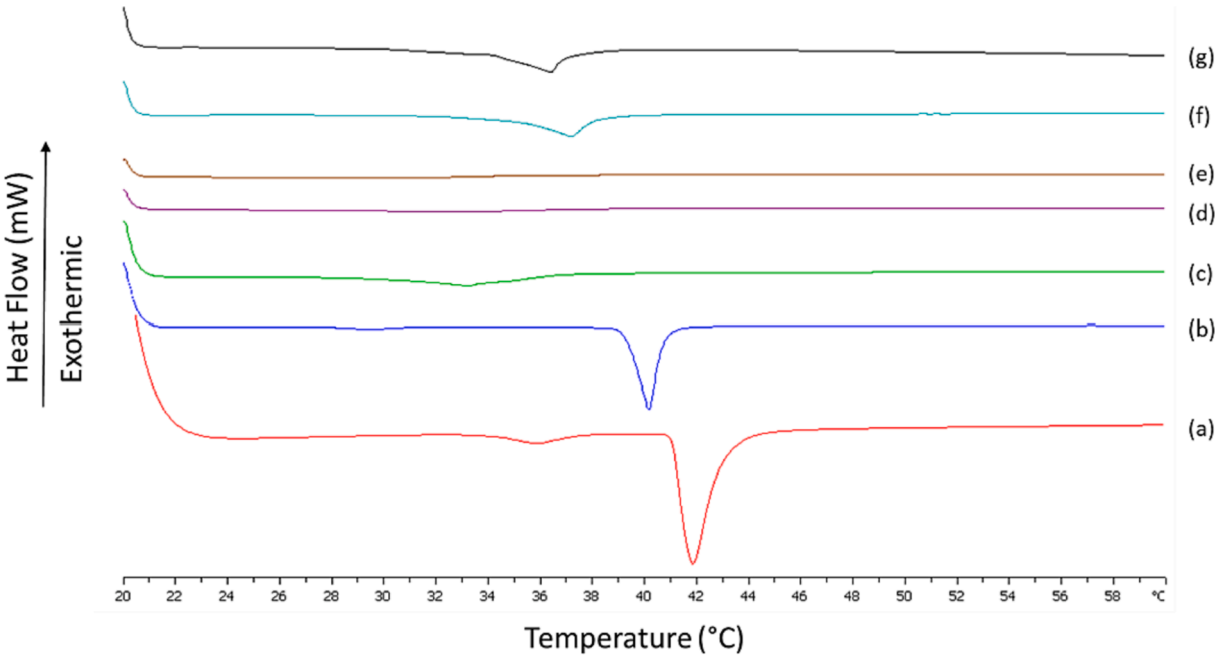

Fig. 7. DSC heating thermograms of (a) DPPC, (b) DPPC:SM 90:10, (c) DPPC:SM:DOPS 75:10:15, (d) DPPC:SM:DOPS:Chol 70:10:15:5, (e) DPPC:SM:DOPS:Chol 65:10:15:10, (f) DPPC:SM:DOPS:Gen 70:10:15:5, and (g) DPPC:SM:DOPS:Gen 65:10:15:10 M ratio lipid bilayers hydrated with HPLC-grade water.

Table 3
Heating calorimetric profiles DPPC, DPPC:SM 90:10, DPPC:SM:DOPS 75:10:15, DPPC:SM:DOPS:Chol 70:10:15:5, DPPC:SM:DOPS:Chol 65:10:15:10, DPPC:SM:DOPS:Gen 70:10:15:5, and DPPC:SM:DOPS:Gen 65:10:15:10 M ratio lipid bilayers hydrated with HPLC-grade water. T_{onset}: temperature at which the thermal event starts; T.: temperature at which heat capacity (ΔCp) at constant pressure is maximum; $\Delta T_{1/2}$: half width at half peak height of the transition; ΔH: transition enthalpy normalized per gram of sample bilayer.

Sample	Molar ratio	T_{onset} °C	T_m °C	$\Delta T_{1/2}$ °C	ΔH J g^{-1}
DPPC	–	40.83	41.49	1.12	41.58
DPPC:SM	90:10	39.20	39.96	0.77	45.98
DPPC:SM:DOPS	75:10:15	29.60	33.19	4.13	30.43
DPPC:SM:DOPS:Chol	70:10:15:5	25.95	33.11	7.17	8.99
DPPC:SM:DOPS:Chol	65:10:15:10	25.63	30.48	6.12	5.43
DPPC:SM:DOPS:Gen	70:10:15:5	34.84	37.11	1.94	37.10
DPPC:SM:DOPS:Gen	65:10:15:10	33.74	36.34	1.97	40.83

(Fritzsching et al., 2013). These lipidic domains have been linked to various cellular processes and influence cellular activities in health and disease (Fantini et al., 2020; Gurung et al., 2021; Levental et al., 2020). Taking into account that the design and composition of the studied lipid bilayers were selected by choosing the key exosomal membrane lipids, we believe that the two rafts that appear in our exosome-like membranes follow the same biophysical formation route as the ones observed in the cellular membranes. The present hypothesis is of high importance as we aim to mimic the unique biophysical properties and consequently, the biological functionality of the exosomal membranes. As to the authors' knowledge, this is the first time that the thermodynamic behavior of an exosomal-like membrane of the current consistency is presented and correlated to cellular and exosomal lipid rafts.

As the obtained thermodynamic data confirmed the formation of the lipid rafts, thermal analysis was further conducted for samples with increased cholesterol or genistein amounts in the bilayer. Although both cholesterol and genistein are small lipophilic molecules (MW_{Chol} = 386.65 g/mol and MW_{Gen} = 270.241 g/mol), their incorporation with the lipid bilayer leads to different structures and fluidity of the membrane. Genistein has three hydroxyl groups (Cao et al., 2013), indicating that its incorporation to the lipid bilayer is focused mainly on the vicinity of the polar head groups of the membrane. In contrast, cholesterol is more lipophilic and is inserted in deeper layers of the bilayer.

In Fig. 7**(d-g)**, the interaction of equimolar mixtures of either cholesterol or genistein within the lipid membrane shows the effect on the thermal behavior of the membrane. The thermal analysis study reveals that cholesterol causes a more intense rearrangement of the membrane as the endothermic ΔH of the bilayers that contain cholesterol is almost zeroed out (8.99 J/g in the case of 5 % mol, and 5.43 J/g for 10 % mol Chol respectively). The T_m is only affected at the highest concentration of Cholesterol, when it shifts down by approximately 3 °C. Regarding genistein, we observe that T_{onset}, T_m, and ΔH values of the endothermic evaluation are higher than the ones of the DPPC:SM:DOPS bilayers, suggesting that genistein is not only a pharmacologically active molecule but can also act as a membrane fluidity factor, too. The tail presented before the T_m indicates the presence of metastable phases (micro-domains) that play a key role for the interactions between the formed nanoparticles and the cellular membranes.

4. Conclusion

Exosome-like nanoparticles composed of DPPC, SM, DOPS, and cholesterol at different molar ratios were developed by either thin-film hydration or microfluidic techniques. The comparative study of the two different preparation methods showed major differences in terms of the obtained particle size of the nanoformulations. The thin-film hydration/sonication method produced smaller exosome-like nanoparticles, with a D_h lower than 100 nm in comparison to Tesla chips. With the thin-film hydration technique, particle size increased as the cholesterol amount increased, while the opposite was observed for the Tesla chips. All of the obtained nanodispersions were stable under storage stability due to the highly negative ζ-potential values. For the loaded genistein into the exosome-like nanoparticles the particle size of the nanoparticles was not affected when using the thin-hydration technique while the Tesla microfluidics presented strong dependence on the genistein content. This behavior is attributed to the effect of the drug molecule on the fluidity of the lipid bilayers. By using Tesla chips, a slightly higher encapsulation efficiency was observed in comparison to lipid-hydration. Thermal analysis showed that the incorporation of genistein resulted in a new thermotropic curve, when compared to the same bilayer without the drug molecule. In conclusion, this is the first time that thin-film hydration and 3D-printed microfluidic protocols were compared for the preparation of non-loaded or genistein-loaded exosome-like nanoparticles. According to the above, we underline that the lipid consistency of the exosome-like nanoparticles has a different effect depending on the method of production. In this study, the Tesla chip appears to be superior for liposomes with high content of cholesterol, as the exosome-like nanoparticles, due to the lower polydispersity index. However, for liposomes with a lower ratio of cholesterol thin film hydration/sonication might be a better method of production. In conclusion, the work demonstrates that novel microfluidic arrays are suitable for the development of complex biomimetic lipid nanoplatforms.

CRediT authorship contribution statement

Maria Tsakiri: . **Atabak Ghanizadeh Tabriz:** . **Nikolaos Naziris:** Investigation, Methodology, Visualization, Writing – original draft. **Kanza Rahali:** Investigation, Methodology. **Dennis Douroumis:** . **Costas Demetzos:** Conceptualization, Project administration, Supervision, Visualization, Writing – original draft.

Declaration of competing interest

The authors declare that they have no known competing financial interests or personal relationships that could have appeared to influence the work reported in this paper.

Data availability

Data will be made available on request.

Acknowledgements

Zetasizer ZSU3105 (Malvern, UK) instrumentation was financed by Uni-Pharma Kleon Tsetis Pharmaceutical Laboratories S.A.

Appendix A. Supplementary material

Supplementary data to this article can be found online at https://doi.org/10.1016/j.ijpharm.2024.123788.

References

Aday, S., Hazan-Halevy, I., Chamorro-Jorganes, A., Anwar, M., Goldsmith, M., Beazley-Long, N., Sahoo, S., Dogra, N., Sweaad, W., Catapano, F., Ozaki-Tan, S., Angelini, G. D., Madeddu, P., Benest, A.V., Peer, D., Emanueli, C., 2021. Bioinspired artificial exosomes based on lipid nanoparticles carrying let-7b-5p promote angiogenesis in vitro and in vivo. Mol. Ther. 29, 2239–2252. https://doi.org/10.1016/j.ymthe.2021.03.015.

Afzal, O., Altamimi, A.S.A., Nadeem, M.S., Alzarea, S.I., Almalki, W.H., Tariq, A., Mubeen, B., Murtaza, B.N., Iftikhar, S., Riaz, N., Kazmi, I., 2022. Nanoparticles in drug delivery: from history to therapeutic applications. Nanomaterials 12. https://doi.org/10.3390/nano12244494.

Ahn, J., Ko, J., Lee, S., Yu, J., Kim, Y., Jeon, N.L., 2018. Microfluidics in nanoparticle drug delivery; From synthesis to pre-clinical screening. Adv. Drug Deliv. Rev. 128, 29–53. https://doi.org/10.1016/j.addr.2018.04.001.

Al-amin, M.D., Bellato, F., Mastrotto, F., Garofalo, M., Malfanti, A., Salmaso, S., Caliceti, P., 2020. Dexamethasone loaded liposomes by thin-film hydration and microfluidic procedures: formulation challenges. Int. J. Mol. Sci. 2020, Vol. 21, Page 1611 21, 1611. https://doi.org/10.3390/IJMS21051611.

Aminu, N., Bello, I., Umar, N.M., Tanko, N., Aminu, A., Audu, M.M., 2020. The influence of nanoparticulate drug delivery systems in drug therapy. J. Drug Delivery Sci. Technol. 60 https://doi.org/10.1016/j.jddst.2020.101961.

Anderson, C.F., Grimmett, M.E., Domalewski, C.J., Cui, H., 2020. Inhalable nanotherapeutics to improve treatment efficacy for common lung diseases. Wiley Interdiscip. Rev. Nanomed. Nanobiotechnol. 12 https://doi.org/10.1002/wnan.1586.

Anselmo, A.C., Mitragotri, S., 2019. Nanoparticles in the clinic: an update. Bioeng. Transl. Med. 4, e10143.

Antonietti, M., Förster, S., 2003. Vesicles and liposomes: a self-assembly principle beyond lipids. Adv. Mater. 15, 1323–1333. https://doi.org/10.1002/adma.200300010.

Aranguren, A., Torres, C.E., Muñoz-Camargo, C., Osma, J.F., Cruz, J.C., 2020. Synthesis of nanoscale liposomes via low-cost microfluidic systems. Micromachines 11, 1–15. https://doi.org/10.3390/mi11121050.

Aryani, A., Denecke, B., 2016. Exosomes as a nanodelivery system: a key to the future of neuromedicine? Mol. Neurobiol. 53, 818–834. https://doi.org/10.1007/s12035-014-9054-5.

Barenholz, Y. (Chezy), 2012. Doxil® — The first FDA-approved nano-drug: Lessons learned. Journal of Controlled Release 160, 117–134. https://doi.org/10.1016/j.jconrel.2012.03.020.

Cao, H., Jing, X., Wu, D., Shi, Y., 2013. Methylation of genistein and kaempferol improves their affinities for proteins. Int. J. Food Sci. Nutr. 64, 437–443. https://doi.org/10.3109/09637486.2012.759186.

Casadó, A., Sagristá, M.L., Mora, M., 2018. A novel microfluidic liposomal formulation for the delivery of the SN-38 camptothecin: Characterization and in vitro assessment of its cytotoxic effect on two tumor cell lines. Int. J. Nanomed. 13, 5301–5320. https://doi.org/10.2147/IJN.S166219.

Chakraborty, R., Parvez, S., 2022. Microfluidics in drug delivery. Microfluidics Multi Organs Chip 135–162. https://doi.org/10.1007/978-981-19-1379-2_6.

Chen, C., Mehl, B.T., Munshi, A.S., Townsend, A.D., Spence, D.M., Martin, R.S., 2016. 3D-printed microfluidic devices: fabrication, advantages and limitations—a mini review. Anal. Methods 8, 6005–6012. https://doi.org/10.1039/C6AY01671E.

Cohen, R., Schwartz, B., Peri, I., Shimoni, E., 2011. Improving bioavailability and stability of genistein by complexation with high-amylose corn starch. J. Agric. Food Chem. 59, 7932–7938. https://doi.org/10.1021/jf2013277.

Costa, A.L.R., Gomes, A., Cunha, R.L., 2017. Studies of droplets formation regime and actual flow rate of liquid-liquid flows in flow-focusing microfluidic devices. Exp. Therm Fluid Sci. 85, 167–175. https://doi.org/10.1016/j.expthermflusci.2017.03.003.

Das, C.K., Jena, B.C., Banerjee, I., Das, S., Parekh, A., Bhutia, S.K., Mandal, M., 2019. Exosome as a novel shuttle for delivery of therapeutics across biological barriers. Mol. Pharm. 16, 24–40. https://doi.org/10.1021/acs.molpharmaceut.8b00901.

Demetzos, C., 2016. Pharmaceutical nanotechnology. Fundamentals and practical applications.

Elsana, H., Olusanya, T.O.B., Carr-wilkinson, J., Darby, S., Faheem, A., Elkordy, A.A., 2019. Evaluation of novel cationic gene based liposomes with cyclodextrin prepared by thin film hydration and microfluidic systems. Sci. Reports 2019 91 9, 1–17. https://doi.org/10.1038/s41598-019-51065-4.

Elvira, K.S., 2021. Microfluidic technologies for drug discovery and development: friend or foe? Trends Pharmacol. Sci. 42, 518–526. https://doi.org/10.1016/j.tips.2021.04.009.

Eskandari, Z., Bahadori, F., Celik, B., Onyuksel, H., 2020. Targeted nanomedicines for cancer therapy, from basics to clinical trials. J. Pharm. Pharm. Sci. 23, 132–157. https://doi.org/10.18433/jpps30583.

Fantini, J., Di Scala, C., Chahinian, H., Yahi, N., 2020. Structural and molecular modelling studies reveal a new mechanism of action of chloroquine and hydroxychloroquine against SARS-CoV-2 infection. Int. J. Antimicrob. Agents 55, 105960. https://doi.org/10.1016/j.ijantimicag.2020.105960.

Fritzsching, K.J., Kim, J., Holland, G.P., 2013. Probing lipid–cholesterol interactions in DOPC/eSM/Chol and DOPC/DPPC/Chol model lipid rafts with DSC and 13C solid-state NMR. Biochimica et Biophysica Acta (BBA) - Biomembranes 1828, 1889–1898. https://doi.org/10.1016/j.bbamem.2013.03.028.

García-Manrique, P., Gutiérrez, G., Blanco-López, M.C., 2018. Fully artificial exosomes: towards new theranostic biomaterials. Trends Biotechnol. 36, 10–14. https://doi.org/10.1016/j.tibtech.2017.10.005.

Gardikis, K., Hatziantoniou, S., Viras, K., Wagner, M., Demetzos, C., 2006. A DSC and Raman spectroscopy study on the effect of PAMAM dendrimer on DPPC model lipid membranes. Int. J. Pharm. 318, 118–123. https://doi.org/10.1016/j.ijpharm.2006.03.023.

Germain, M., Caputo, F., Metcalfe, S., Tosi, G., Spring, K., Åslund, A.K.O., Pottier, A., Schiffelers, R., Ceccaldi, A., Schmid, R., 2020. Delivering the power of nanomedicine to patients today. J. Control. Release 326, 164–171. https://doi.org/10.1016/j.jconrel.2020.07.007.

Gleason, C.E., Fischer, B.L., Dowling, N.M., Setchell, K.D.R., Atwood, C.S., Carlsson, C. M., Asthana, S., 2015. Cognitive effects of soy isoflavones in patients with Alzheimer's disease. J. Alzheimer's Disease 47, 1009–1019. https://doi.org/10.3233/JAD-142958.

Gurung, S., Perocheau, D., Touramanidou, L., Baruteau, J., 2021. The exosome journey: from biogenesis to uptake and intracellular signalling. Cell Commun. Signal. 19, 47. https://doi.org/10.1186/s12964-021-00730-1.

Hirohata, M., Ono, K., Takasaki, J., Takahashi, R., Ikeda, T., Morinaga, A., Yamada, M., 2012. Anti-amyloidogenic effects of soybean isoflavones in vitro: Fluorescence spectroscopy demonstrating direct binding to Aβ monomers, oligomers and fibrils. Biochimica et Biophysica Acta (BBA) - Molecular Basis of Disease 1822, 1316–1324. https://doi.org/10.1016/j.bbadis.2012.05.006.

Kalluri, R., LeBleu, V.S., 2020. The biology, function, and biomedical applications of exosomes. Science 367. https://doi.org/10.1126/science.aau6977.

Karnik, R., Gu, F., Basto, P., Cannizzaro, C., Dean, L., Kyei-Manu, W., Langer, R., Farokhzad, O.C., 2008. Microfluidic platform for controlled synthesis of polymeric nanoparticles. Nano Lett. 8, 2906–2912. https://doi.org/10.1021/nl801736q.

Leekumjorn, S., Cho, H.J., Wu, Y., Wright, N.T., Sum, A.K., Chan, C., 2009. The role of fatty acid unsaturation in minimizing biophysical changes on the structure and local effects of bilayer membranes. Biochimica et Biophysica Acta (BBA) - Biomembranes 1788, 1508–1516. https://doi.org/10.1016/j.bbamem.2009.04.002.

Leung, A.K.K., Tam, Y.Y.C., Chen, S., Hafez, I.M., Cullis, P.R., 2015. Microfluidic mixing: a general method for encapsulating macromolecules in lipid nanoparticle systems. J. Phys. Chem. B 119, 8698–8706. https://doi.org/10.1021/acs.jpcb.5b02891.

Levental, I., Levental, K.R., Heberle, F.A., 2020. Lipid rafts: controversies resolved, mysteries remain. Trends Cell Biol. 30, 341–353. https://doi.org/10.1016/j.tcb.2020.01.009.

Li, Y.-J., Wu, J.-Y., Liu, J., Xu, W., Qiu, X., Huang, S., Hu, X.-B., Xiang, D.-X., 2021. Artificial exosomes for translational nanomedicine. J. Nanobiotechnol. 19 https://doi.org/10.1186/s12951-021-00986-2.

Magarkar, A., Dhawan, V., Kallinteri, P., Viitala, T., Elmowafy, M., Róg, T., Bunker, A., 2014. Cholesterol level affects surface charge of lipid membranes in saline solution. Sci. Rep. 4, 5005. https://doi.org/10.1038/srep05005.

Martins, J.P., das Neves, J., de la Fuente, M., Celia, C., Florindo, H., Günday-Türeli, N., Popat, A., Santos, J.L., Sousa, F., Schmid, R., Wolfram, J., Sarmento, B., Santos, H.A., 2020. The solid progress of nanomedicine. Drug Delivery and Translational Research 10, 726–729. https://doi.org/10.1007/s13346-020-00743-2.

Mas-Bargues, C., Borrás, C., Viña, J., 2022. The multimodal action of genistein in Alzheimer's and other age-related diseases. Free Radic. Biol. Med. 183, 127–137. https://doi.org/10.1016/j.freeradbiomed.2022.03.021.

Matsingou, C., Hatziantoniou, S., Georgopoulos, A., Dimas, K., Terzis, A., Demetzos, C., 2005. Labdane-type diterpenes: thermal effects on phospholipid bilayers, incorporation into liposomes and biological activity. Chem. Phys. Lipids 138, 1–11. https://doi.org/10.1016/j.chemphyslip.2005.07.006.

Mitchell, M.J., Billingsley, M.M., Haley, R.M., Wechsler, M.E., Peppas, N.A., Langer, R., 2021. Engineering precision nanoparticles for drug delivery. Nat. Rev. Drug Discov. 20, 101–124. https://doi.org/10.1038/s41573-020-0090-8.

Nakhaei, P., Margiana, R., Bokov, D.O., Abdelbasset, W.K., Jadidi Kouhbanani, M.A., Varma, R.S., Marofi, F., Jarahian, M., Beheshtkhoo, N., 2021. Liposomes: Structure, Biomedical Applications, and Stability Parameters With Emphasis on Cholesterol. Frontiers in Bioengineering and Biotechnology 9.

Petry, F. dos S., Hoppe, J.B., Klein, C.P., dos Santos, B.G., Hözer, R.M., Bifi, F., Matté, C., Salbego, C.G., Trindade, V.M.T., 2021. Genistein attenuates amyloid-beta-induced cognitive impairment in rats by modulation of hippocampal synaptotoxicity and hyperphosphorylation of Tau. The Journal of Nutritional Biochemistry 87, 108525. https://doi.org/10.1016/j.jnutbio.2020.108525.

Rebollo, R., Oyoun, F., Corvis, Y., El-Hammadi, M.M., Saubamea, B., Andrieux, K., Mignet, N., Alhareth, K., 2022. Microfluidic manufacturing of liposomes: development and optimization by design of experiment and machine learning. ACS Appl. Mater. Interfaces 14, 39736–39745. https://doi.org/10.1021/acsami.2c06627.

Roces, C.B., Lou, G., Jain, N., Abraham, S., Thomas, A., Halbert, G.W., Perrie, Y., 2020. Manufacturing considerations for the development of lipid nanoparticles using microfluidics. Pharmaceutics 12, 1–19. https://doi.org/10.3390/pharmaceutics12111095.

Sahu, T., Ratre, Y.K., Chauhan, S., Bhaskar, L.V.K.S., Nair, M.P., Verma, H.K., 2021. Nanotechnology based drug delivery system: current strategies and emerging therapeutic potential for medical science. J. Drug Delivery Sci. Technol. 63, 102487 https://doi.org/10.1016/j.jddst.2021.102487.

Sarfraz, M., Afzal, A., Yang, T., Gai, Y., Raza, S.M., Khan, M.W., Cheng, Y., Ma, X., Xiang, G., 2018. Development of dual drug loaded nanosized liposomal formulation by a reengineered ethanolic injection method and its pre-clinical pharmacokinetic studies. Pharmaceutics 10. https://doi.org/10.3390/pharmaceutics10030151.

Seo, E.-J., Fischer, N., Efferth, T., 2018. Phytochemicals as inhibitors of NF-κB for treatment of Alzheimer's disease. Pharmacol. Res. 129, 262–273. https://doi.org/10.1016/j.phrs.2017.11.030.

Sercombe, L., Veerati, T., Moheimani, F., Wu, S.Y., Sood, A.K., Hua, S., 2015. Advances and challenges of liposome assisted drug delivery. Front. Pharmacol. 6.

Skotland, T., Sandvig, K., Llorente, A., 2017. Lipids in exosomes: current knowledge and the way forward. Prog. Lipid Res. 66, 30–41. https://doi.org/10.1016/j.plipres.2017.03.001.

Skupin-Mrugalska, P., Zalewski, T., Elvang, P.A., Nowaczyk, G., Czajkowski, M., Piotrowska-Kempisty, H., 2021. Insight into theranostic nanovesicles prepared by thin lipid hydration and microfluidic method. Colloids Surfaces B Biointerfaces 205, 111871. https://doi.org/10.1016/J.COLSURFB.2021.111871.

Sommonte, F., Weaver, E., Mathew, E., Denora, N., Lamprou, D.A., 2022. In-house innovative “Diamond Shaped" 3D printed microfluidic devices for lysozyme-loaded liposomes. Pharmaceutics. https://doi.org/10.3390/pharmaceutics14112484.

Tabriz, A.G., Viegas, B., Okereke, M., Uddin, M.J., Lopez, E.A., Zand, N., Ranatunga, M., Getti, G., Douroumis, D., 2022. Evaluation of 3D printability and biocompatibility of microfluidic resin for fabrication of solid microneedles. Micromachines 13. https://doi.org/10.3390/mi13091368.

Tesla, N., 1920. Valvular Conduit. 1 (329), 559.

Thapa, R.K., Kim, J.O., 2023. Nanomedicine-based commercial formulations: current developments and future prospects. J. Pharm. Investig. 53, 19–33. https://doi.org/10.1007/s40005-022-00607-6.

Théry, C., Zitvogel, L., Amigorena, S., 2002. Exosomes: composition, biogenesis and function. Nat. Rev. Immunol. 2, 569–579. https://doi.org/10.1038/nri855.

Tiboni, M., Tiboni, M., Pierro, A., Del Papa, M., Sparaventi, S., Cespi, M., Casettari, L., 2021. Microfluidics for nanomedicines manufacturing: an affordable and low-cost 3D printing approach. Int. J. Pharm. 599 https://doi.org/10.1016/j.ijpharm.2021.120464.

Trajkovic, K., Hsu, C., Chiantia, S., Rajendran, L., Wenzel, D., Wieland, F., Schwille, P., Brügger, B., Simons, M., 2008. Ceramide triggers budding of exosome vesicles into multivesicular endosomes. Science 319, 1244–1247. https://doi.org/10.1126/science.1153124.

Trandum, C., Westh, P., Jørgensen, K., Mouritsen, O.G., 2000. A thermodynamic study of the effects of cholesterol on the interaction between liposomes and ethanol. Biophys. J. 78, 2486–2492. https://doi.org/10.1016/S0006-3495(00)76793-2.

Tsakiri, M., Naziris, N., Demetzos, C., 2021. Innovative vaccine platforms against infectious diseases: under the scope of the COVID-19 pandemic. Int. J. Pharm. 610, 121212 https://doi.org/10.1016/j.ijpharm.2021.121212.

Tsakiri, M., Naziris, N., Mahairaki, V., Demetzos, C., 2022a. Artificial exosomes as targeted drug delivery systems. Nanotechnol. Life Sci. 123–147. https://doi.org/10.1007/978-3-031-12658-1_5.

Tsakiri, M., Peraki, A., Chountoulesi, M., Demetzos, C., 2022b. Chimeric liposomes decorated with P407: an alternative biomaterial for producing stealth nano-therapeutics. J. Liposome Res. 32, 83–91. https://doi.org/10.1080/08982104.2021.1978486.

Uppal, S., Italiya, K.S., Chitkara, D., Mittal, A., 2018. Nanoparticulate-based drug delivery systems for small molecule anti-diabetic drugs: an emerging paradigm for effective therapy. Acta Biomater. 81, 20–42. https://doi.org/10.1016/j.actbio.2018.09.049.

Vhora, I., Lalani, R., Bhatt, P., Patil, S., Misra, A., 2019. Lipid-nucleic acid nanoparticles of novel ionizable lipids for systemic BMP-9 gene delivery to bone-marrow mesenchymal stem cells for osteoinduction. Int. J. Pharm. 563, 324–336. https://doi.org/10.1016/j.ijpharm.2019.04.006.

Waghule, T., Saha, R.N., Singhvi, G., 2023. Exploring microfluidics and membrane extrusion for the formulation of temozolomide-loaded liposomes: investigating the effect of formulation and process variables. J. Liposome Res. 33, 170–182. https://doi.org/10.1080/08982104.2022.2139844.

Wang, J., Shao, C., Wang, Y., Sun, L., Zhao, Y., 2020. Microfluidics for medical additive manufacturing. Engineering 6, 1244–1257. https://doi.org/10.1016/j.eng.2020.10.001.

Weaver, E., Mathew, E., Caldwell, J., Hooker, A., Uddin, S., Lamprou, D.A., 2023. The manufacturing of 3D-printed microfluidic chips to analyse the effect upon particle size during the synthesis of lipid nanoparticles. J. Pharm. Pharmacol. 75, 245–252. https://doi.org/10.1093/jpp/rgac085.

Zhang, L., Chen, Q., Ma, Y., Sun, J., 2020. Microfluidic methods for fabrication and engineering of nanoparticle drug delivery systems. ACS Appl. Bio Mater. 3, 107–120. https://doi.org/10.1021/acsabm.9b00853.

Zhao, C.-X., 2013. Multiphase flow microfluidics for the production of single or multiple emulsions for drug delivery. Adv. Drug Deliv. Rev. 65, 1420–1446. https://doi.org/10.1016/j.addr.2013.05.009.

Zhao, L., Feng, S.-S., Kocherginsky, N., Kostetski, I., 2007. DSC and EPR investigations on effects of cholesterol component on molecular interactions between paclitaxel and phospholipid within lipid bilayer membrane. Int. J. Pharm. 338, 258–266. https://doi.org/10.1016/j.ijpharm.2007.01.045.